

# Multipolarization Dynamic Light Scattering of Nonspherical Nanoparticles in Solution

Alexander D. Levin,<sup>\*,†</sup> Ekaterina A. Shmytkova,<sup>+</sup> and Boris N. Khlebtsov<sup>#</sup>

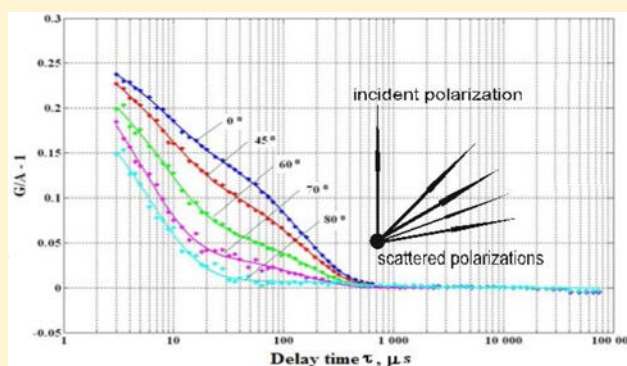
<sup>†</sup>All-Russian Research Institute for Optical and Physical Measurements, 46 Ozernaya street, Moscow, 119361 Russia

<sup>#</sup>Institute of Biochemistry and Physiology of Plants and Microorganisms Russian Academy of Sciences, 13 Prospect Entuziastov, Saratov, 410049, Russia

## Supporting Information

**ABSTRACT:** Application of dynamic light scattering (DLS) for sizing of non-spherical nanoparticles using copolarized and cross-polarized components of the scattered light is limited by the difficulties of measurement of very weak cross-polarized light intensity and problems with inverting of the scattering data into direct prediction of nanoparticles size parameters. Here we propose the new technique, called multipolarization DLS, based on time-resolved measurements of the scattered light intensity at different angles between the incident and scattered light polarizations. The physical model giving the relation between particle's translational and rotational diffusion coefficients and intensity autocorrelation function (ACF) for the arbitrary angle between the incident and scattered polarizations is developed.

Numerical algorithm for the inverse problem of calculating the diffusion coefficients from the family of ACFs is introduced, and a semiempirical approach for length and diameter estimation of quasi-cylindrical nanoparticles from the diffusion coefficients is proposed. The application to Au and Fe<sub>2</sub>O<sub>3</sub> nanorods, in particular to monitor the selective etching-induced size changing, is described. In comparison with depolarized DLS, the method allows one to avoid measurement of the very weak cross-polarized component of the scattered light, and gives more data for solving the inverse problem of size parameter reconstruction from the scattered light intensity.



## INTRODUCTION

Nonspherical nanoparticles, such as nanorods, nanowires, and nanotubes, have received much attention due to their unique optical properties and due to their applications in nanoelectronics, nanophotonics, solar batteries, nanocomposite materials, and biomaterials.<sup>1–4</sup> The wet chemical approach provides the most effective way to synthesize large amounts of high-quality anisotropic nanoparticles. Thus, noninvasive techniques for rapidly monitoring the geometrical parameters of nonspherical nanoparticles are of great interest.<sup>5–7</sup> Depolarized dynamic light scattering (DLS) is a known sizing technique for nonspherical nanoparticles. The presence of a depolarized component in the light scattering signal allows both the translational and rotational diffusion of nonspherical nanoparticles to be assessed. As a result, depolarized DLS provides not only the hydrodynamic radius of the equivalent sphere but also the actual length and diameter of diffusing nanoparticles. By considering nanoparticle Brownian motion in the terms of translational and rotational diffusion, the particle dimensions can be determined by the decay rates of the fluctuations of the scattered light. Decay rates are determined for the light scattered with two different polarizations, one of which (copolarization) aligns with the polarization of the exciting light (VV), and the other (cross-polarization) is

perpendicular to it (VH). The scattered light collection system includes a polarization analyzer, which is switched between two fixed positions, one of them transmitting the VV light, and the other the VH light. Then the intensity autocorrelation functions (ACF)  $G_{VV}^{(2)}(\tau)$  and  $G_{VH}^{(2)}(\tau)$ , where  $\tau$  is the ACF delay time, are calculated from the time dependences of the scattered light intensity. These ACFs are related to the nanoparticles translational and rotational diffusion coefficients  $D_{trans}$  and  $D_{rot}$ . The particle length  $L$  and diameter  $d$  can be found from the values of the diffusion coefficients using the diffusion model for particles of a given shape (e.g., cylindrical). Using depolarized DLS measurements, the size parameters of Au nanorods<sup>8–11</sup> and single wall<sup>12,13</sup> and multiwall<sup>14</sup> carbon nanotubes have been studied. However, wider application of depolarized DLS to characterizing nonspherical nanoparticles have been limited by intrinsic challenges in measuring typically weak cross-polarized scattering signals and by the difficulties of inverting experimental ACFs of the scattered light into direct predictions of nanoparticles dimensions.<sup>11</sup>

Received: October 10, 2016

Revised: January 12, 2017

Published: January 12, 2017

To weaken both of these limitations, we proposed an improved DLS approach called multipolarization dynamic light scattering (MP DLS). A preliminary brief description of the technique is given in an SPIE conference paper,<sup>15</sup> and its application to the carbon nanotubes size estimation is described in ref 16. This article presents a detailed description of the method and introduces its physical foundations. It also describes the new algorithm of data processing and implementation together with the experimental results of nonspherical nanoparticles sizing and etching-induced size changing.

## I. THEORETICAL BASIS

Basically, the idea of the proposed method is to measure the time dependence of scattered intensity at several analyzer positions intermediate between VV and VH, i.e., with different angles between the incident and scattered polarization directions. Thus, the equation relating the ACF of the scattered light with the arbitrary polarization direction should be derived.

We used Pecora's theory<sup>17</sup> for the spectrum of the light scattered by optically anisotropic molecules. According to this theory, the power spectral density of the light scattered by optically anisotropic particles  $I(q, \omega)$  can, in the general case, be represented as the sum of the isotropic and anisotropic components:

$$I(q, \omega) = I_{\text{iso}}(q, \omega) + I_{\text{aniso}}(q, \omega) \quad (1)$$

Note that the theory takes into account intermolecular motion. We can simplify the problem by assuming the particle to be rigid, i.e., by ignoring the relative motion of its parts. We will also assume the particles to be axially symmetric, implying that

$$I_{\text{iso}}(q, \omega) = \frac{\rho}{2\pi} \cdot K^2 \cdot \cos^2(\varphi) \cdot \sin^2(\psi) \cdot \alpha_{\perp}^2 \cdot P(q) \cdot S_{\text{iso}}(q, \omega) \quad (2)$$

$$I_{\text{aniso}}(q, \omega) = \frac{\rho}{30\pi} \cdot K^2 \cdot [3 + \cos^2(\varphi) \cdot \sin^2(\psi)] \cdot S_{\text{aniso}}(q, \omega) \quad (3)$$

where  $q$  is the scattering vector

$$q = \frac{4\pi n \sin\left(\frac{\theta}{2}\right)}{\lambda} \quad (4)$$

Here and below,  $n$  is the refractive index of the liquid,  $\theta$  is the scattering angle, and  $\lambda$  is the laser wavelength.  $\omega$  is the Doppler shift of the laser light frequency due to the motion of the particles,  $\rho$  is the number concentration of particles,  $K$  is a parameter depending on the intensity of the incident light and the distance from the scattering volume to the detector,

$$\alpha_{\perp} = (2\alpha_{\perp} + \alpha_{\parallel}) \quad (5)$$

$\alpha_{\parallel}$  ( $\alpha_{\perp}$ ) is the polarizability for the electric field along (perpendicular to) the cylinder axis,  $\psi$  is the angle between the scattered light wave vector and the incident polarization vector (in most DLS setups, the incident polarization vector is orthogonal to the scattering plane, so  $\psi = 90^\circ$ ),  $\varphi$  is the angle between the polarization vector of the scattered light and the plane formed by the scattered light wave vector and the incident polarization vector (this angle depends on the rotation angle of the Glan–Thompson prism, which varies from  $0^\circ$  in the vertical position VV to  $90^\circ$  in the horizontal position VH).

$P(q)$  is the so-called “form factor”, a particle shape dependent function of the wave vector. Formulas 2 and 3 involve dynamic structural factors  $S_{\text{iso}}(q, \omega)$  and  $S_{\text{aniso}}(q, \omega)$ , which are expressed as follows in terms of the translational and rotational diffusion coefficients:

$$S_{\text{iso}}(q, \omega) = \frac{2q^2 D_{\text{trans}}}{\omega^2 + (q^2 D_{\text{trans}})^2} \quad (6)$$

$$S_{\text{aniso}}(q, \omega) = Y \frac{2(q^2 D_{\text{trans}} + 6D_{\text{rot}})}{\omega^2 + (q^2 D_{\text{trans}} + 6D_{\text{rot}})^2} \quad (7)$$

where  $Y = (\alpha_{\perp} - \alpha_{\parallel})^2/3$ , and  $D_{\text{trans}} = (D_{\perp} + D_{\parallel})/2$  is the average translational diffusion coefficient, with  $D_{\perp}$  and  $D_{\parallel}$  being the diffusion coefficients perpendicular and parallel to the cylinder axis, respectively, and  $D_{\text{rot}}$  is the rotational diffusion coefficient.

According to the Wiener–Khinchin theorem,<sup>18</sup> the first-order autocorrelation function  $G^{(1)}$  of a stationary random process is related to the spectral density by the Fourier transform. Performing this transformation, and remembering that  $\sin(\psi) = 1$ , we obtain

$$G^{(1)}(\tau) = \frac{\rho}{2\pi} K^2 \left\{ \cos^2(\varphi) \cdot \alpha_{\perp}^2 \cdot P(q) \cdot \exp[-(q^2 \cdot D_{\text{t}}) \tau] + \frac{3 + \cos^2(\varphi)}{15} \cdot Y \cdot \exp[-(q^2 \cdot D_{\text{t}} + 6D_{\text{r}}) \tau] \right\} \quad (8)$$

which, when normalized to its value at  $\tau = 0$ , yields

$$g^{(1)}(\tau) = \frac{G^{(1)}(\tau)}{G^{(1)}(0)} = A \cdot \exp[-(q^2 \cdot D_{\text{t}}) \tau] + B \cdot \exp[-(q^2 \cdot D_{\text{t}} + 6D_{\text{r}}) \tau] \quad (9)$$

where

$$A = \frac{\cos^2(\varphi) \cdot \alpha_{\perp}^2 \cdot P(q)}{\cos^2(\varphi) \cdot \alpha_{\perp}^2 \cdot P(q) + \frac{3 + \cos^2(\varphi)}{15} \cdot Y} \quad (10)$$

and

$$B = 1 - A \quad (11)$$

It can be shown that in the two limiting cases ( $\varphi = 0$  in the VV geometry, and  $\varphi = 90^\circ$  in the VH geometry) eq 9 leads to the conventional depolarized DLS formulas.<sup>9</sup> For an arbitrary value of  $\varphi$ , eq 10 can be written as

$$A(\varphi) = \frac{A(0)}{1 + A(0) \cdot C \cdot \tan^2(\varphi)} \quad (12)$$

where

$$A = \frac{\alpha_{\perp}^2}{\alpha_{\perp}^2 + 3 \cdot Y} = \alpha_{\perp}^2 / [\alpha_{\perp}^2 + (\alpha_{\perp} - \alpha_{\parallel})^2] \quad (13)$$

$$C = \frac{1}{5} \frac{Y}{\alpha_{\perp}^2 P(q)} = \frac{1}{15} \frac{(\alpha_{\parallel} - \alpha_{\perp})^2}{\alpha_{\perp}^2 P(q)} \quad (14)$$

The second-order ACF  $G^{(2)}(\tau)$  measured by the DLS instrument is related to the first-order ACF (eq 9) by the Siegert relation<sup>19</sup>

Table 1. Nanoparticle Size Parameters Determined from TEM and LSPR

sample name	TEM data			LSPR data	
	length, nm	diameter, nm	aspect ratio	peak wavelength, nm	aspect ratio
Au_Alfa_1	40.7 ± 1.5	16.1 ± 0.1	2.5 ± 0.1	788	3.6
Au_Alfa_2	44.4 ± 1.8	11.6 ± 0.4	3.8 ± 0.3	838	4.1
Au_custom_1	76.1 ± 1.8	14.5 ± 0.3	5.2 ± 0.2	931	5.0
Au_custom_2	79.7 ± 7.5	14.5 ± 1.6	4.7 ± 1.6	1055	6.2
Fe <sub>2</sub> O <sub>3</sub> _custom	458.3 ± 16.6	72.7 ± 2.1	6.3 ± 0.4	--	--

$$G^{(2)}(\varphi, \tau) = G^{(2)}(\varphi, 0) \cdot [1 + \beta(\varphi) \cdot |g^{(1)}(\varphi, \tau)|^2] \quad (15)$$

where  $G^{(2)}(\varphi, 0)$  is the ACF baseline, and  $\beta(\varphi)$  is the instrument dependent factor known as the “intercept”.

Formulas 9, 11, 12, and 15 give the solution of the direct problem, i.e., the intensity ACF for a nanoparticle suspension with given values of the diffusion coefficients and an arbitrary angle between the incident and scattered light polarizations. These formulas were used to solve the inverse problem of MP DLS, i.e., the calculation of the translational and rotational diffusion coefficients from the family of ACF measured for different values of  $\varphi$ . The solution algorithm for inverse problem will be presented below in section III.

## II. EXPERIMENTAL SECTION

The developed method was applied to the sizing of several Au nanorod suspensions and a suspension of hematite (Fe<sub>2</sub>O<sub>3</sub>) rods and to the size-changing of the Au nanorods due to selective etching. For estimation purposes and for comparison of MP DLS results, all the samples were also studied by transmission electron microscopy (TEM), and for the Au nanorods, the extinction spectra were measured in the spectral range around the localized surface plasmon resonance (LSPR) peak.

**Materials.** Two commercially available suspensions of Au nanorods, purchased from Alfa Aesar, were studied. Additionally, two samples of Au nanorods with different geometrical and optical properties were synthesized and studied.

The suspensions of positively charged Au nanorods with nominal length of 46–56 nm and diameter of 9–15 nm (product # 46810, lot J18 × 003, further called Au\_Alfa\_1) and those of negatively charged Au nanorods 55–65 nm in length and 9–15 nm in diameter (product # 46972, lot L05 × 008, further called Au\_Alfa\_2).

**Synthesizing Au Nanorods.** All chemicals obtained from commercial suppliers were used in the synthesis process without further purification. Cetyltrimethylammonium bromide (CTAB, > 98.0%), sodium oleate (C<sub>18</sub>H<sub>33</sub>NaO<sub>2</sub> technical grade >82% fatty acid), L-ascorbic acid (AA, > 99.9%), hydrochloric acid (HCl, 37 wt % in water), and sodium borohydride (NaBH<sub>4</sub>, 99%) were purchased from Sigma-Aldrich. Hydrogen tetrachloroaurate trihydrate (HAuCl<sub>4</sub>·3H<sub>2</sub>O) and silver nitrate (AgNO<sub>3</sub>, > 99%) were purchased from Alfa Aesar. Ultrapure water obtained from a Milli-Q Integral 5 system was used in all experiments.

High-yield Au nanorod solution was prepared in binary surfactant mixture using a method described previously.<sup>20,21</sup> At the first step, a seed solution of 2–3 nm particles was prepared by adding 0.025 mL of 10 mM HAuCl<sub>4</sub> into 1 mL of aqueous 0.1 M CTAB, followed by the addition of 1 mL of 10 mM NaBH<sub>4</sub> solution. The seed solution was aged at room temperature for 90 min before use in the next step.

To prepare the growth solution, 0.7 g of CTAB and 0.123 g of sodium oleate were dissolved in 25 mL water (~50 °C). The solution was first allowed to cool down to 30 °C and then 2.4 mL of 4 mM AgNO<sub>3</sub> solution was added. The mixture was kept undisturbed at 30 °C for 15 min after which 25 mL of 1 mM HAuCl<sub>4</sub> solution was added. The solution became colorless after 90 min of stirring, indicating the reduction of Au<sup>3+</sup> to Au<sup>+</sup>. Then 0.3 mL of HCl (37 wt %) was introduced to adjust the pH value of the growth solution. After another 15 min, 0.125 mL of 64 mM ascorbic acid and 0.08 or 0.04 mL (depending on the geometrical parameters of the nanorods) of the seed solution was added. The resultant mixture was left undisturbed at 30 °C for 48 h for Au nanorods growth. As prepared Au nanorods were centrifuged at 7000g for 20 min and a pellet was resuspended in water to obtain a final Au concentration of 0.5 mM. Nanoparticle lengths and diameters at the synthesized suspensions were controlled using TEM and the LSPR extinction spectrum peaks. The two samples, further called Au\_custom\_1 and Au\_custom\_2, were synthesized by the techniques described above.

**Selective Etching.** Selective etching of Au nanorods was performed for the testing of MP DLS size tracking opportunity. The samples used for etching were Au\_Alfa\_1, Au\_Alfa\_2 and Au\_custom\_2. The 10 and 20 μL 0.2% HAuCl<sub>4</sub> solution was added to 1 mL of Au nanorods to carry out the etching process.

**Synthesizing Fe<sub>2</sub>O<sub>3</sub> Nanorods.** Monodisperse spindle-shaped hematite particles with controllable aspect ratios were fabricated by forced hydrolysis of ferric chloride solutions. Hematite particles were prepared by aging 100 mL of aqueous solution containing 2.0 × 10<sup>-2</sup> M FeCl<sub>3</sub> and 4.0 × 10<sup>-4</sup> M KH<sub>2</sub>PO<sub>4</sub> at 100 °C for 72 h. The resulting precipitate was centrifuged and washed several times with water and ethanol. Finally, the precipitate was resuspended in 25 mL ethanol.

**Extinction and TEM Measurements.** The extinction spectra of Au nanorods were measured using double beam photometer-fluorimeter SFF-2 «FLUORAN» (VNII OFI, Russia) and are presented in Figure S1 (Supporting Information (SI)). LSPR peaks are clearly observed for each spectrum.

TEM measurements were performed using FEI Tecnai F20 G2 S-TWIN microscope with a 200 kV accelerating voltage. For TEM imaging, the drop containing nanoparticles was dried on a special grid. For each sample, TEM images are presented in Figure S2 (SI). Image processing was made using ImageJ software.<sup>22</sup>

**MP DLS Measurements.** MP DLS measurements were carried out using a nanoparticle size analyzer «ARN-2» developed by VNII OFI (Russia) and described in ref 15. A single-mode 12 mW HeNe laser with a linearly polarized output (polarization ratio 500:1) is used as a light source, and scattering angles could be set in the range from 15° to 165°. Scattered light collection system includes a Glan-Tompson prism with the adjustable angle of rotation  $\varphi$ . An Avalanche

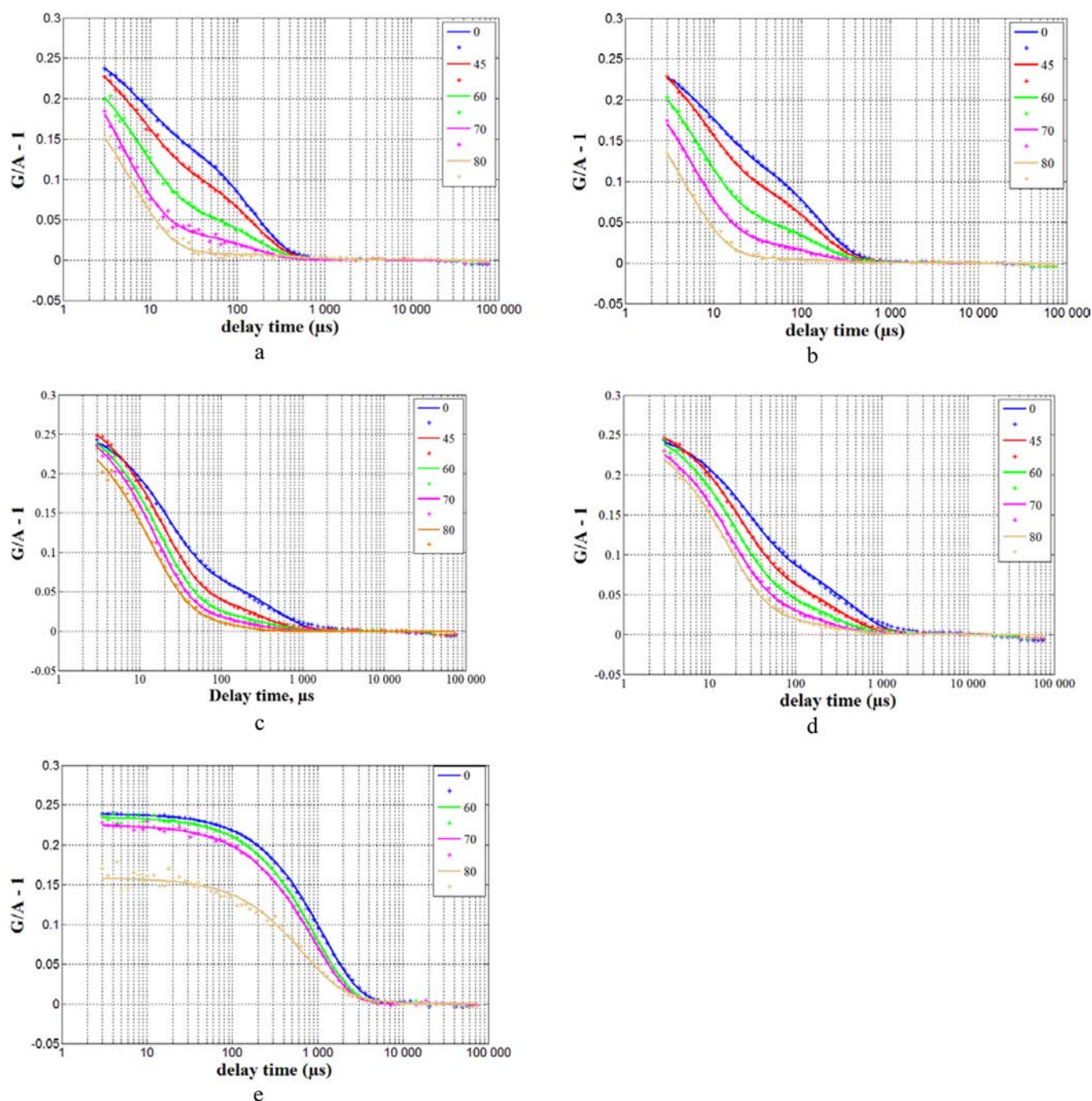


**Figure 1.** ACF families (series of measurements at different angles between incident and scattered polarizations) (a) Au\_Alfa\_1,  $\theta = 90^\circ$ ; (b) Au\_Alfa\_2,  $\theta = 90^\circ$ ; (c) Au\_custom\_1,  $\theta = 75^\circ$ ; (d) Au\_custom\_2,  $\theta = 75^\circ$ ; (e) Fe<sub>2</sub>O<sub>3</sub>\_custom,  $\theta = 75^\circ$ .

photodiode photon counting module with a 100  $\mu\text{m}$  active area diameter was applied as a photodetector. A fast real-time software correlator based on a multitau algorithm<sup>23</sup> was used in ACF calculations.

Prior to the MP DLS measurement, all samples were diluted and vortexed for 5 min using a vibrational Henschel Reax top shaker. Measurements were made in a cylindrical cell. During MP DLS measurements, intensity ACFs were measured for the scattering angles of  $75^\circ$  and  $90^\circ$ ; for each scattering angle, measurements were performed for several values of the angle  $\varphi$  as defined by the position of the Glan–Thomson prism. The most often used set of  $\varphi$  values included  $0^\circ$ ,  $45^\circ$ ,  $60^\circ$ , and  $70^\circ$ .

### III. RESULTS AND DISCUSSION

**TEM and LSPR Results.** Nanoparticles size parameters determined from TEM images and LSPR spectra are presented in Table 1. Approximately 100 particles were counted for each sample in order to determine the average length and values presented.

**MP DLS Data Processing.** From the family of experimental ACF, the diffusion coefficients  $D_{\text{trans}}$  and  $D_{\text{rot}}$  and several three auxiliary parameters [ $G^{(2)}(\varphi, 0)$ ,  $\beta(\varphi)$ , and  $A(0)$ ] were calculated by a nonlinear least-squares (NLLS) fitting procedure using eqs 9, 11, 12, and 15. For each ACF there are five fitting parameters and about 70 ACF values for different delay times. Thus, the problem is over-determined,

making the Levenberg–Marquardt algorithm preferred over other NNLS procedures.<sup>24</sup> Data processing by the algorithms presented above was performed using custom functions written for Matlab (Mathworks, USA). Examples of ACF measured for Au nanorods are shown in Figure 1a–d.

In all figures, the dots present the experimental ACF values, and the dashed lines present ACF calculated using eqs 9, 11, 12, and 15 with the fitting parameter values.

The ACF approximation error can be estimated as

$$\delta = \frac{\sum_{i=1}^N [G_{\text{exper}}(\tau_i) - G_{\text{calc}}(\tau_i)]^2}{\lim_{\tau \rightarrow \infty} G_{\text{calc}}(\tau)} \quad (16)$$

where  $G_{\text{exper}}(\tau_i)$  and  $G_{\text{calc}}(\tau_i)$  are the measured and calculated ACF, respectively, and  $\tau_i$  is the delay time values for which ACF was measured. The nominator in eq 16 represents the norm of residuals—the main measure of fitting quality.

For the processing of all ACF presented in this paper,  $\delta$  is less than 0.05. The values of  $D_{\text{trans}}$  and  $D_{\text{rot}}$  calculated from ACF with the different values of  $\varphi$  were averaged with the weights proportional to  $1/\delta$ . The details of the calculation procedure, the solution stability analysis with respect to noise, and the description of Matlab code are presented in the SI. The translational and rotational diffusion coefficients calculated from the experimental ACF are given in Table 2.

**Calculation of Nanoparticles Length and Diameter from the Diffusion Coefficients.** In calculating the length  $L$  and diameter  $d$ , a diffusion model for particles in a solution<sup>25–30</sup> should be used with the values of  $D_{\text{trans}}$  and  $D_{\text{rot}}$  obtained.

In virtually all models, formulas for the coefficients of the translational and rotational diffusion can be reduced to the form

$$D_{\text{trans}} = \frac{kT}{3\pi\eta L} [\ln P + C_{\text{trans}}(P)] \quad (17)$$

$$D_{\text{rot}} = \frac{3kT}{\pi\eta L^3} [\ln P + C_{\text{rot}}(P)] \quad (18)$$

where  $k$  is the Boltzmann constant,  $T$  is the absolute temperature in K,  $\eta$  is the dynamic viscosity of the solvent,  $P = L/d$  is the aspect ratio,  $C_{\text{trans}}$  and  $C_{\text{rot}}$  are the (aspect-ratio-dependent) correction factors for the translational and rotational diffusion, respectively, that take into account the finite length effects at the ends of the cylinder.

Different theories describing the diffusion of cylindrical particles in a liquid give different correction factors. In the simplest case with  $C_{\text{trans}} = C_{\text{rot}} = 0$ , and the model reduces to the classical theory of Kirkwood.<sup>25</sup> Such model was used by Eitoku et al.<sup>14</sup> for processing depolarized DLS data on multiwall carbon nanotubes. More sophisticated models propose various expressions for the correction factors  $C_{\text{trans}}$  and  $C_{\text{rot}}$ . The Tirado and Garcia de la Torre (TG) model<sup>26,27</sup> was used by Rodriguez-Fernandez et al.,<sup>9</sup> Glidden and Martin,<sup>11</sup> and Haghghi et al.<sup>28</sup> to calculate gold nanorods length and diameter from  $D_{\text{trans}}$  and  $D_{\text{rot}}$  determined using depolarized DLS. The model of Broersma<sup>29,30</sup> was applied by Reddy et al.<sup>10</sup> to Au nanorods, and Brenner's model<sup>31</sup> for rigid cylindrical rods was applied by Shetty et al.<sup>13</sup> and Hirroi et al.<sup>32</sup> to single-wall carbon nanotubes. In almost all models,  $C_{\text{trans}}$  and  $C_{\text{rot}}$  are functions of the inverse aspect ratio  $1/P$ .

The formulas that take into account cylinder end effects are different in different models, and in addition to that, the rod shape is in most cases different from an ideal cylinder. Thus, the accurate calculation of size parameters from the translational

Table 2. Nanorod Parameters Determined from MP DLS in Comparison with TEM and Extinction Data

sample	length, nm			diameter, nm			aspect ratio				
	$D_{\text{trans}}/\mu^2\text{s}^{-1}$	$D_{\text{rot}}/\text{ms}^{-1}$	MP DLS	TEM	$L_{\text{DLS}}/L_{\text{TEM}}$	MP DLS	TEM	$d_{\text{DLS}}/d_{\text{TEM}}$	MP DLS	TEM	LSPR
Au_Alfa_1	8.85 ± 0.44	18.08 ± 0.9	66.4 ± 3.5	40.7 ± 1.5	1.63 ± 0.15	19.9 ± 1.2	16.1 ± 0.1	1.25 ± 0.08	3.3 ± 0.4	2.5 ± 0.1	3.6
Au_Alfa_2	9.98 ± 0.50	17.47 ± 0.87	71.7 ± 3.7	44.4 ± 1.8	1.62 ± 0.15	16.5 ± 1.6	11.6 ± 0.4	1.42 ± 0.19	4.3 ± 0.6	3.8 ± 0.3	4.1
Au_custom_1	6.21 ± 0.31	6.27 ± 0.31	94.3 ± 5.0	76.1 ± 1.8	1.24 ± 0.09	28.4 ± 2.0	14.5 ± 0.3	1.96 ± 0.18	3.8 ± 0.4	5.2 ± 0.2	5.0
Au_custom_2	6.48 ± 0.32	5.91 ± 0.29	99.3 ± 5.1	79.7 ± 7.5	1.25 ± 0.18	26.6 ± 2.2	14.5 ± 1.6	1.80 ± 0.35	3.7 ± 0.5	4.7 ± 1.6	6.2
Fe <sub>3</sub> O <sub>3</sub> _custom	1.49 ± 0.07	0.35 ± 0.02	197.3 ± 8.5	458.3 ± 16.6	0.430 ± 0.03	59.0 ± 3.8	72.7 ± 2.1	0.81 ± 0.08	3.4 ± 0.4	6.3 ± 0.4	†

and rotational diffusion coefficients by means of purely theoretical models is problematic. Therefore, we restrict ourselves to approximate estimates based on the above-mentioned Kirkwood model,<sup>25</sup> which neglects the end effects. These estimates are presented in Table 2 in comparison with the TEM data. For the diffusion coefficients and length and diameter values, the standard uncertainties are presented. Also presented in the table are the values of the Au nanorods aspect ratio calculated from the LSPR extinction spectrum peaks.

Nanorod aspect ratio  $P$  can be estimated from the values of the peak wavelength  $\lambda_{\text{LSPR}}$  using the formula<sup>33</sup> ( $\lambda_{\text{LSPR}}$  in nanometers)

$$P = 0.0098 \cdot \lambda_{\text{LSPR}} - 4.12 \quad (19)$$

The values thus obtained from MP DLS data can be considered as the length and diameter of the *equivalent cylinder*, which has the same translational and rotational diffusion coefficients as the particle being measured. The proposed concept of an equivalent cylinder can be regarded as an extension of the concept of equivalent sphere widely used in particle sizing.<sup>34</sup> The length and diameter of the equivalent cylinder can be used for the monitoring of nanoparticles stability in liquid media and for the time-resolved monitoring of size variation due to various physical or chemical processes. An example of such monitoring is presented below.

Table 2 also presents the MP DLS/TEM length and diameter ratios. Two distinct groups of the Au nanorods can be recognized: Alfa Asear rods (Au\_Alfa\_1 and Au\_Alfa\_2) and customized rods (Au\_custom1 and Au\_custom2). Within each group, the MP DLS/TEM length and diameter ratios are very close to each other. This is likely due to the fact that the rods in one group were synthesized by the same technology and are similar in morphology. The ratios mentioned above can be used as correction factors in semiempirical model of diffusion coefficients and used for matching the MP DLS and TEM data.

For the Fe<sub>2</sub>O<sub>3</sub> nanorods, the discrepancy between MP DLS and TEM data is much higher. This is because the shape of nanorod differs considerably from a cylinder.

**Comparison of MP DLS with the Conventional Depolarized DLS.** We made the additional measurements with the gold nanorods suspension for the comparison of the two methods. For this sample we used both the conventional depolarized DLS ( $\varphi = 0^\circ$  and  $90^\circ$ ) and MP DLS ( $\varphi = 0^\circ$ ,  $45^\circ$ ,  $60^\circ$  and  $70^\circ$ ). It should be noticed that for measuring the acceptable quality ACF for  $\varphi = 90^\circ$  the concentration of nanoparticles in suspension should be rather high (for gold nanorods exceeds three times or more that for  $\varphi = 70^\circ$ ).

The comparison of the results presented in Table 3 and Figure 2 show that data developed within the MP DLS method gives better characteristics in measurement error and more

accurate results for the aspect ratio than the conventional depolarized DLS.

**Control of the Etching-Induced Size Changing.** It is observed that Au nanorods change their size and shape when etched. For each sample, the ACF were measured by the MP DLS procedure described above in section II. The measurements were made first before etching and then about 1 h after etching. After each MP DLS measurement, the extinction spectra were measured. Data processing was made as described above.

Figure 3 shows the ACF families obtained for one of the samples before and after etching.

All results of etching size changing are presented in Table 4.

It can be noticed that for the positively charged nanorods (Au\_Alfa\_1 and Au\_custom\_2), the etching process reduces the length and increase the diameter. There is some literature<sup>35–37</sup> on the effect of etching on the length and diameter of Au nanorods, most of which reports a decrease in the rod aspect ratio, which sometimes<sup>35</sup> implies a decrease in length with no change in diameter and sometimes,<sup>37</sup> a decrease in length and increase in diameter. It should be noted that etching did not change the length and diameter of the negatively charged nanorods (in contrast to those positively charged). The dependence of physical and chemical transformations of Au nanorods on their charge was pointed out recently.<sup>38</sup> It can also be seen from the data in Table 4 that for the positively charged nanorods, the etching-induced reduction in the aspect ratio as detected from the shift of the LSPR peak is approximately consistent with the nanorod length reduction measured using MP DLS. It can be hypothesized that the MP DLS-measured etching-induced increase in the nanorod diameter occurs due to the formation around the nanorod surface of the ion shell, which does not significantly affect the LSPR extinction spectrum peak. Such a shell could be formed due to adsorption of AuCl<sub>4</sub><sup>−</sup> anions on the positively charged nanorod surface. Thus, the shell increased in DLS-measured hydrodynamic diameter but did not change in LSPR- and TEM-measured diameter values.

#### IV. CONCLUSION

In summary, a new DLS-based method expanding the possibilities for sizing nonspherical particles in liquid media has been developed. The method is based on the time-resolved intensity measurements of light scattered by nanoparticles for various angles between the incident and scattered polarization directions. A theoretical model of scattered intensity ACF at arbitrary angles between incident and scattered polarizations and nonlinear algorithm for calculating the translational and rotational diffusion coefficients from the family of experimental ACFs have been developed.

The Au nanorods and Fe<sub>2</sub>O<sub>3</sub> rods were under experimental study. The particle lengths and diameters estimated from the diffusion coefficients using a simple Kirkwood diffusion model for Au nanorods are in qualitative agreement with TEM data; the greater discrepancy for Fe<sub>2</sub>O<sub>3</sub> rods is due to the significant shape distinction from a cylinder. The concept of an equivalent cylinder having the same translational and rotational diffusion coefficients as the particle being measured was proposed for the sizing of axisymmetric nonspherical nanoparticles. The concept can be useful for monitoring nanoparticle stability in liquid media and for the time-resolved observation of size variations. That was demonstrated by the size changing of Au nanorods in the process of selective etching.

**Table 3. Comparison of MP DLS and Conventional Depolarized DLS Results**

	depolarized DLS	MP DLS	LSPR
$D_{\text{trans}}, \mu^2\text{s}^{-1}$	$7.27 \pm 0.72$	$8.52 \pm 0.43$	
$D_{\text{rot}}, \text{ms}^{-1}$	$18.3 \pm 1.8$	$17.2 \pm 0.8$	
$L, \text{nm}$	$59.7 \pm 7.0$	$66.8 \pm 3.4$	
$d, \text{nm}$	$24.5 \pm 2.1$	$20.8 \pm 1.3$	
aspect ratio	2.44	3.21	3.6

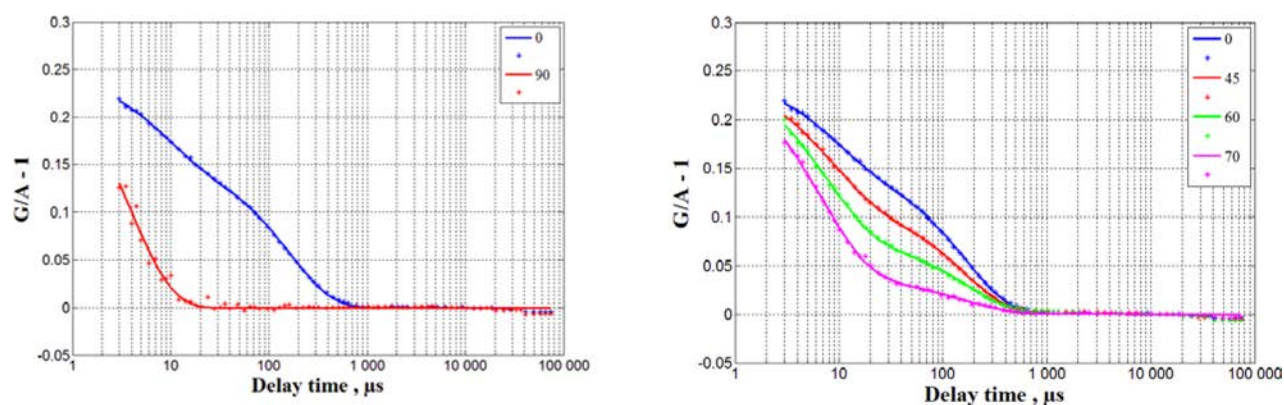


Figure 2. ACF measured for the gold nanorods suspension (data presented in Table 2), using (a) conventional depolarized DLS and (b) MP DLS.

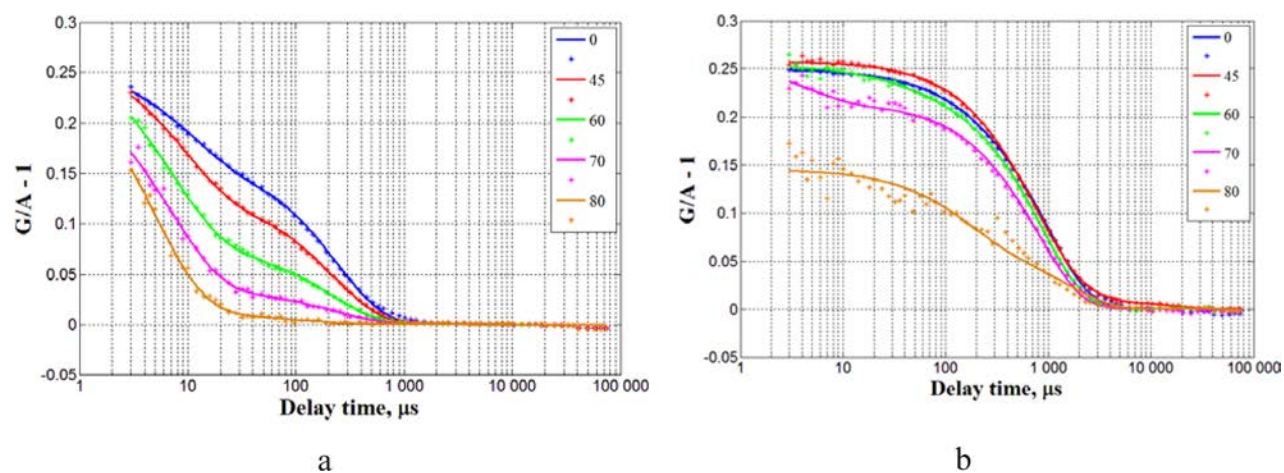


Figure 3. ACF families (series of measurements at different angles between incident and scattered polarizations) for Au nanorods (Au\_Alfa\_1) before and after etching, 75° scattering angle.

Table 4. Variation of Nanorod Parameters after Etching

sample	HAuCl <sub>4</sub> volume in 1 sm <sup>3</sup> etching solution, μL	length, nm		diameter, nm		MP DLS length reduction	LSPR aspect ratio reduction
		before etching	after etching	before etching	after etching		
Au_Alfa_1 (+ charged)	5	70.9 ± 3.5	50.6 ± 2.5	18.1 ± 1.1	41.2 ± 2.5	1.4	1.1
Au_Alfa_2 (- charged)	5	78.1 ± 3.9	77.2 ± 3.9	11.8 ± 1.1	13.4 ± 1.3	1.01	1.0
Au_custom_2 (+ charged)	10	102.1 ± 5.2	68.4 ± 3.5	24.3 ± 2.0	39.4 ± 3.2	1.5	1.4

In comparison with conventional depolarized DLS, the new technique avoids the measurement of very weak cross-polarized component of the scattered light, thereby reducing either the power of the incident laser light or the number concentration of nanoparticles in the liquid and increasing the amount of experimental data available for solving of the inverse problem. Also, this technique, due to the increased amount of experimental data, opens up the opportunity to calculate not only the average values of nanoparticle length and diameter but also their distribution over polymodal nanoparticle systems.

## ■ ASSOCIATED CONTENT

### Supporting Information

The Supporting Information is available free of charge on the ACS Publications website at DOI: 10.1021/acs.jpcc.6b10226.

Nanoparticle TEM images, extinction spectra with plasmon resonance peaks, the description of the Matlab code calculating of nonspherical nanoparticle diffusion coefficients, and size parameters from the set of the measured autocorrelation functions of the scattered light intensity (PDF)

## ■ AUTHOR INFORMATION

### Corresponding Author

\*E-mail: ad\_levin@mail.ru; Tel. +7 495 781 24 55.

### ORCID

Alexander D. Levin: 0000-0001-9087-952X

### Notes

The authors declare no competing financial interest.

## ACKNOWLEDGMENTS

Financial support from the Ministry of Education and Science of the Russian Federation in the framework of the project RFMEFI62414X0009 is acknowledged. The authors are grateful to Ivan Zhovannik for the help with graphic design.

## REFERENCES

- (1) Sau, T. K.; Rogach, A. L.; Jackel, F.; Klar, T. A.; Feldmann, J. Properties and applications of colloidal nonspherical noble metal nanoparticles. *Adv. Mater.* **2010**, *22*, 1805–1825.
- (2) Zhang, Ch.; Yan, Y.; Zhao, Y. Sh.; Yao, J. Synthesis and applications of organic nanorods, nanowires and nanotubes. *Annu. Rep. Prog. Chem., Sect. C: Phys. Chem.* **2013**, *109*, 211–239.
- (3) Ibrahim, K. S. Carbon nanotubes—properties and applications: a review. *Carbon Lett.* **2013**, *14*, 131–144.
- (4) Meyer, R. A.; Green, J. J. Shaping the future of nanomedicine: anisotropy in polymeric nanoparticle design. *WIREs Nanomedicine and Nanotechnology* **2016**, *8*, 191–207.
- (5) Mathaes, R.; Winter, G.; Engert, J.; Besheer, A. Application of different analytical methods for the characterization of non-spherical micro- and nanoparticles. *Int. J. Pharm.* **2013**, *453*, 620–629.
- (6) Zhang, B.; Lan, T.; Huang, X.; Dong, C.; Ren, J. Sensitive single particle method for characterizing rapid rotational and translational diffusion and aspect ratio of anisotropic nanoparticles and its application in immunoassays. *Anal. Chem.* **2013**, *85*, 9433–9438.
- (7) Wang, A.; Dimiduk, T. J.; Fung, J.; Razavi, S.; Kretzschmar, I.; Chaudhary, K.; Manoharan, V. N. Using the discrete dipole approximation and holographic microscopy to measure rotational dynamics of non-spherical colloidal particles. *J. Quant. Spectrosc. Radiat. Transfer* **2014**, *146*, 499–509.
- (8) Lehner, D.; Lindner, H.; Glatter, O. Determination of the translational and rotational diffusion coefficients of rodlike particles using depolarized dynamic light scattering. *Langmuir* **2000**, *16*, 1689–1695.
- (9) Rodriguez-Fernandez, J.; Pérez-Juste, J.; Liz-Marzán, L. M.; Lang, P. R. Dynamic light scattering of short Au rods with low aspect ratios. *J. Phys. Chem. C* **2007**, *111*, 5020–5025.
- (10) Reddy, N. K.; Pérez-Juste, J.; Pastoriza-Santos, I.; Lang, P. R.; Dhont, J. K.; Liz-Marzán, L. M.; Vermant, J. Flow dichroism as a reliable method to measure the hydrodynamic aspect ratio of gold nanoparticles. *ACS Nano* **2011**, *5*, 4935–4944.
- (11) Glidden, M.; Muschol, M. Characterizing gold nanorods in solution using depolarized dynamic light scattering. *J. Phys. Chem. C* **2012**, *116*, 8128–8137.
- (12) Badaire, S.; Poulin, P.; Maugey, M.; Zakri, C. In situ measurements of nanotube dimensions in suspensions by depolarized dynamic light scattering. *Langmuir* **2004**, *20*, 10367–10370.
- (13) Shetty, A. M.; Wilkins, G. M. H.; Nanda, J.; Solomon, M. J. Multiangle depolarized dynamic light scattering of short functionalized single-walled carbon nanotubes. *J. Phys. Chem. C* **2009**, *113*, 7129–7133.
- (14) Eitoku, T.; Tange, M.; Kato, H.; Okazaki, T. Depolarized dynamic light scattering study of multi-walled carbon nanotubes in solutions. *Mater. Express* **2013**, *3*, 37–42.
- (15) Levin, A. D.; Shmytkova, E. A. Nonspherical nanoparticles characterization using partially depolarized dynamic light scattering. *Proc. SPIE* **2015**, *9526*, 95260 P1–95260 P8.
- (16) Levin, A. D.; Lobach, A. S.; Shmytkova, E. A. Study of geometric parameters of nonspherical nanoparticles by partially depolarized dynamic light scattering. *Nanotechnol. Russ.* **2015**, *10*, 400–407.
- (17) Pecora, R. Spectrum of light scattered from optically anisotropic macromolecules. *J. Chem. Phys.* **1968**, *49*, 1036–1043.
- (18) Goodman, J. W. *Statistical Optics*; Wiley: Hoboken, NJ, 2000.
- (19) Frisken, B. J. Revisiting the method of cumulants for the analysis of dynamic light-scattering data. *Appl. Opt.* **2001**, *40*, 4087–4091.
- (20) Ye, X.; Zheng, Chen, J.; Gao, Y.; Murray, C. B. Using binary surfactant mixtures to simultaneously improve the dimensional tunability and monodispersity in the seeded growth of gold nanorods. *Nano Lett.* **2013**, *13*, 765–771.
- (21) Khlebtsov, B. N.; Khanadeev, V. A.; Ye, J.; Sukhorukov, G. B.; Khlebtsov, N. G. Overgrowth of gold nanorods by using a binary surfactant mixture. *Langmuir* **2014**, *30*, 1696–1703.
- (22) Image J User Guide, available from the USA National Institutes of Health: <http://rsb.info.nih.gov/ij>.
- (23) Magatti, D.; Ferri, F. Fast multi-tau software correlator for dynamic light scattering. *Appl. Opt.* **2001**, *40*, 4011–4021.
- (24) More, J. J. The Levenberg-Marquardt algorithm: implementation and theory. Numerical analysis, ed. Watson, G. A., Ed.; Lecture notes in mathematics 630; Springer Verlag: Berlin, 1977, pp 105–116.
- (25) Kirkwood, J. G. The general theory of irreversible processes in solutions of macromolecules. *J. Polym. Sci.* **1954**, *12*, 1–14.
- (26) Tirado, M. M.; Martinez, C. L.; Garcia de la Torre, J. Comparison of theories for the translational and rotational diffusion coefficients of rodlike macromolecules. Application to short DNA fragments. *J. Chem. Phys.* **1984**, *81*, 2047–2052.
- (27) Ortega, A.; Garcia de la Torre, J. Hydrodynamic properties of rodlike and disklike particles in dilute solution. *J. Chem. Phys.* **2003**, *119*, 9914–9919.
- (28) Haghighi, M.; Plum, M. A.; Gantzounis, G.; et al. Plasmon enhanced dynamic Depolarized Light Scattering. *J. Phys. Chem. C* **2013**, *117*, 8411–8419.
- (29) Broersma, S. Viscous force constant for a closed cylinder. *J. Chem. Phys.* **1964**, *32*, 1632.
- (30) Broersma, S. Viscous force and torque constants for a cylinder. *J. Chem. Phys.* **1981**, *74*, 6989–6990.
- (31) Brenner, H. Rheology of a dilute suspension of axisymmetric brownian particles. *Int. J. Multiphase Flow* **1974**, *1*, 195–341.
- (32) Hiroi, T.; Ata, S.; Shibayama, M. Transitions of aggregation states for concentrated carbon nanotube dispersion. *J. Phys. Chem. C* **2016**, *120*, 5776–5782.
- (33) Khlebtsov, B. N.; Khanadeev, V. A.; Khlebtsov, N. G. Extinction and extra-high depolarized light scattering spectra of gold nanorods with improved purity and dimension tunability: direct and inverse problems. *Phys. Chem. Chem. Phys.* **2014**, *16*, 5710–5722.
- (34) Schärfl, W. *Light Scattering from Polymer Solutions and Nanoparticle Dispersions*; Springer: Berlin, 2007; Vol. XIV, p 191.
- (35) Khanadeev, V. A.; Burov, A. M.; Khlebtsov, N. G.; Khlebtsov, B. N. Tuning of plasmon resonance of gold nanorods by controlled etching. *Colloid J.* **2015**, *77*, 652–660.
- (36) Alex, S. A.; Satija, J.; Khan, A. M.; Bhalerao, G. M.; Chakravarty, S.; Kasilingam, B.; Sivakumar, A.; Chandrasekaran, N.; Mukherjee, A. Etching-based transformation of dumbbell-shaped gold nanorods facilitated by hexavalent chromium and their possible application as a plasmonic sensor. *Anal. Methods* **2015**, *7*, 5583–5592.
- (37) Wen, T.; Zhang, H.; Tang, X.; Chu, W.; Liu, W.; Ji, Y.; Hu, Z.; Hou, S.; Hu, X.; Wu, X. Copper ion assisted reshaping and etching of gold nanorods: mechanism studies and applications. *J. Phys. Chem. C* **2013**, *117*, 25769–25777.
- (38) Umar, A.; Choi, S. M. Aggregation behavior of oppositely charged gold nanorods in aqueous solution. *J. Phys. Chem. C* **2013**, *117*, 11738–11743.